Materials Science & Engineering C 92 (2018) 374–380

Contents lists available at ScienceDirect

Materials Science & Engineering C

journal homepage: www.elsevier.com/locate/msec

Optimization of strontium aluminate-based mechanoluminescence materials for occlusal examination of artificial tooth

Yanjiao Jiang[a,b], Fu Wang[b], Hui Zhou[b], Zengjie Fan[a], Chen Wu[b], Jie Zhang[a], Bin Liu[a,*], Zhaofeng Wang[b,*]

[a] School of Stomatology, Lanzhou University, Lanzhou, Gansu 730000, China
[b] State Key Laboratory of Solid Lubrication, Lanzhou Institute of Chemical Physics, Chinese Academy of Sciences, Lanzhou, Gansu 730000, China

ARTICLE INFO

Keywords:
Mechanoluminescence
Strontium aluminate
Composites
Occlusal examination

ABSTRACT

This work presents a novel approach for evaluating the occlusal examination of artificial tooth based on the mechanoluminescence (ML) materials. The rare earth doped strontium aluminate ($SrAl_2O_4$: Eu^{2+}, Dy^{3+}; SAOED) was chosen as the ML material, which was further composited with the commercial denture base resin (DBR) to determine its feasibility for the mechanics analysis of artificial tooth occlusion. To eliminate negative factors for occlusal analysis, SAOED was first optimized to exhibit a rapid decay of afterglow and enhanced ML intensity. The luminescent characterizations of the SAOED/DBR composites suggest DBR is a desirable elastic-supporter for nondestructive ML generation. Furthermore, the introduction of SAOED improved the mechanical performance of DBR, and its biocompatibility was maintained at the same time. These results suggest the feasibility of the idea to detect the mechanics in occlusal examination of artificial tooth based on ML. The bright and sensitive ML from the constructed standard artificial tooth models could guide clinicians to purposefully adjust the occlusal surface until a balanced occlusion established.

1. Introduction

Dentition defect is a common oral-maxillofacial disease, which will further arouse a series of complications (e.g., temporomandibular joint disorder, decreased masticatory efficiency, alveolar bone atrophy, etc.) if there is no artificial tooth applied [1, 2]. In addition to the properties of artificial tooth itself, the occlusal-articulation of the filled tooth is crucial adjective in clinic [3, 4]. The inappropriate occlusion of the artificial tooth would also result in dysfunction of the oral-maxillofacial system and temporomandibular joints. An accurate identification of the occlusal high points and interference points of artificial tooth is prerequisite for the establishment of a correct occlusion in clinic [5]. At present, articulating paper is widely employed as a diagnostic tool for occlusal analysis of dental practice [5, 6]. It is extensively accepted that occlusal contact point and occlusal load could be exhibited by the mark size and spot of articulating paper [7]. Generally, the occlusal area with greater contact pressure represents markings with darker color. Although articulating paper is able to record occlusion information, it suffers the problems of low sensitivity and inaccuracy which have received increasing attention [8]. In some recent researches [9, 10], they even showed that the relationship between the color of contact area of articulating paper and contact force was reversed compared with the usually recognized one. Therefore, it is highly required to develop a more reliable approach to detect mechanics of artificial tooth during occlusal test.

Mechanoluminescence (ML) is a type of luminescence produced by mechanical stimuli, e.g., grinding, impact, rub, press and stretching [11]. The phenomenon of ML has been known for centuries. However, it is only in recent years that ML has attracted much attention [12–14]. This is because most of the previously observed ML belongs to destructive luminescence, showing limited application prospect. Since the non-destructive elastico-mechanoluminescence was realized by Xu et al. in 1999 [15], much more researches about ML have been carried out, and a series of advanced applications based on ML have been explored, e.g., stress sensor [16], flexible handwriting device [17], and wind-driven displaying device [18]. Since ML materials could be driven by various mechanical stimuli and the oral environment is filled with mechanics and friction, the combination of ML materials and artificial tooth is supposed to be an effective approach to respond to the mechanics information for occlusal analysis.

Inspired by the above consideration, we applied ML materials for articulating test in this work. The rare earth doped strontium aluminate ($SrAl_2O_4$: Eu^{2+}, Dy^{3+}; SAOED) was employed as the ML component because of its bright and sensitive ML, as well as the excellent chemical

* Corresponding authors.
E-mail addresses: liubkq@lzu.edu.cn (B. Liu), zhfwang@licp.cas.cn (Z. Wang).

https://doi.org/10.1016/j.msec.2018.06.056
Received 25 September 2017; Received in revised form 18 May 2018; Accepted 26 June 2018

and physical stability [16, 19]. In addition, compared with the sulfide-based ML materials [20, 21], SAOED is environmentally friendly and non-toxic, which is much more suitable for oral occlusion application. It should be noted that SAOED is also a typical long-lasting phosphor which could emit light for hundreds of hours after removing the irradiation source [22]. Such afterglow behavior goes against the occlusal analysis. To eliminate the interference from afterglow, the concentration and trap depths in structure were regulated first via adjusting the chemical composition of SAOED. The optimized SAOED showed rarely afterglow after removing the irradiation source just for 20 s, while its ML intensity was greatly enhanced. The optimized SAOED was then composited with the widely used denture base resin (DBR). The investigation results suggest that the introduction of SAOED in DBR could not only emit intense ML, but also exhibit good biocompatibility and enhanced mechanical and tribological performance. The construction of oral standard models based on the SAOED/DBR composite further demonstrates the feasibility of ML materials for occlusal analysis.

2. Experimental details

2.1. Synthesis of SAOED

$Sr_{1-x-y}Al_2O_4$: xEu^{2+}, yDy^{3+} (x = 0.01, 0.02, 0.03, 0.04, y = 0, 0.01, 0.02, 0.03) was synthesized via a solid-state reaction. For each sample of $Sr_{1-x-y}Al_2O_4$: xEu^{2+}, yDy^{3+}, the total amount was set to 0.05 mol. First, stoichiometric $SrCO_3$ (99%), Al_2O_3 (99%), Eu_2O_3 (99.99%), and Dy_2O_3 (99.99%) were mixed and thoroughly ground in an agate mortar with the assistance of ethanol. Then, the mixture was transferred to an alumina crucible and sintered in a tube furnace (GSL-1600X, Hefei Ke Jing Material Technology Co., Ltd.) at 1300 °C for 4 h under reducing atmosphere (90% N_2/10% H_2). After cooling to room temperature, the reacted sample were collected and ground for later use.

2.2. Synthesis of SAOED/epoxy resin composites

To achieve non-destructive elastico-ML for characterization and optimization, the as-synthesized SAOED were composited with epoxy resin. SAOED and epoxy resin were mixed with a weight ratio of 1:7. The mixture was mechanically stirred in a beaker, and then poured into a customized spherical mold with size of 25 mm in diameter and 20 mm in thickness. Finally, the mixture was solidified under 60 °C for 2 h in an oven and the SAOED/epoxy resin composite was obtained.

2.3. Synthesis of SAOED/DBR composites

SAOED/DBR composites were prepared for evaluating the feasibility of ML materials for mechanics detection of artificial tooth. SAOED and the commercial DBR powder (composed of 99% polymethyl methacrylate powder and 1% benzoyl peroxide) were first mixed with a certain weight ratio in an agate mortar. After thoroughly ground with an appropriate amount of ethanol, the mixture powder was transferred to a beaker, and methyl methacrylate monomer was added with half weight of the powder. In order to prepare samples with size of 25 mm in diameter and 20 mm in thickness for ML tests, the mixture was transferred to a customized mold and cured under room temperature for 1 h. The composites prepared with the SAOED to DBR weight ratios of 1:8, 1:7, 1:6 and 1:5 were named to S1-D8, S1-D7, S1-D6 and S1-D5, respectively. The artificial tooth models were fabricated by employing a denture mold, and the other procedures were same with those of SAOED/DBR composites.

2.4. MTT assay

The SAOED/DBR composites with size of 10 × 10 × 2 mm were sterilized under ultraviolet (UV) radiation for overnight and used for cell cultures. L929 Fibroblasts (a clonal mouse fibroblasts cell line, ATCC, Rockville, MD, USA) were employed to evaluate the biocompatibility and proliferation behaviors of the prepared SAOED/DBR composites. The fibroblasts L929 cells were cultured at a density of 10^4 cells per sample in Dulbecco's modified Eagle's medium (DMEM, Gibco, USA) supplemented with fetal bovine serum (FBS, 10%, Australia Origin, Gibco, USA), Penicillin-Streptomycin (100 UI mL^{-1}) and D-glucose (4.5 g L^{-1}) under 5% aseptic CO_2 atmosphere and the temperature of 37 °C. The media was refreshed every two days until the cells reached confluence. Then, the composites were placed into a 24-well plate and seeded with 10^4 cell/mL concentration on each well. At a given time (1, 2 and 4 days), 100 μL of 3-(4,5-dimethyl-2-thiazolyl)-2,5-diphenyl-2-H-tetrazolium bromide (MTT, St. Louis, MO, USA) solution was injected into each well. The cells were cultured for another 4 h. The lower blue formazan reaction product was dissolved by adding 750 μL of dimethylsulfoxide. Then, the mixed solution was transferred into a 96-well plate, and its absorbance was measured by a microplate reader (Bio-Rad iMark) for three times for calculating the average absorbance value. For comparison, the absorbance of the cells only in the culture medium was selected as control. The proliferation performance of the as-prepared samples was obtained by comparing the absorbance of experiment group and control group.

2.5. Characterizations

The crystal structure of SAOED was studied by X-Ray Diffraction (XRD, D/max-2400, Rigaku, Cu-Kα). The absorption spectra were collected by a UV–visible (UV–vis) spectrophotometer (PE lamda 950, USA) using $BaSO_4$ as a reference. The photoluminescence (PL) spectra and decay curves were measured by a fluorescence spectrophotometer (Omni-λ300i, Zolix, China). The ML performance were tested using a ML test system built by Lanzhou Institute of Chemical Physics that consists of electronic universal testing machine (WDT-5, Tian Shui Hong Shan Testing Machine New Technology Development Co., Ltd), rotary tribometer (MS-T3001, Lanzhou Huahui Instrument Technology Co., Ltd.), and photomultiplier tubes and data collection system (DCS103, Zolix, China).

The tribological properties of the SAOED/DBR composites was evaluated using a CSM reciprocating tribometer at ambient conditions (RH = 30 ± 5%). A GCr15 bearing steel ball with a diameter of 6 mm was used as the counterpart. The reciprocating frequency and stroke were 0.5 Hz and 5 mm, respectively. The normal force was selected as 10 N. The coefficient of friction and sliding passes were recorded automatically.

The wear rates of composites after the tests were calculated as follows:

$$W = \frac{V}{L \times D}$$

where W, V, L and D represent wear rate, wear volume, applied load and sliding distance, respectively. The cross-sectional area of the thickness of the samples was measured by Alpha-Step D-100 profilemeter (KLA-Tencor, San Francisco, CA). The hardness of composite is presented with Shore A durometer. Three replicate tests were carried out for each specimen.

3. Results and discussion

The crystal structure of monoclinic $SrAl_2O_4$ with space group of $P2_1$ is illustrated in Fig. 1a. In the unit cell, there are three independent cation sites for Eu^{2+} and Dy^{3+} doping, i.e., two nine-coordinated Sr^{2+} sites and one four-coordinated Al^{3+} site. Because of the radius difference among Eu^{2+} (0.117 nm), Dy^{3+} (0.091 nm), Sr^{2+} (0.118 nm) and Al^{3+} (0.053 nm), it is suggested that Eu^{2+} and Dy^{3+} ions should substitute the sites of Sr^{2+} ions in SAOED [23, 24]. The crystal phase of the as-prepared SAOED powder was determined by XRD, as shown in Fig. 1b. It is observed that the XRD patterns of SAOED is identical with

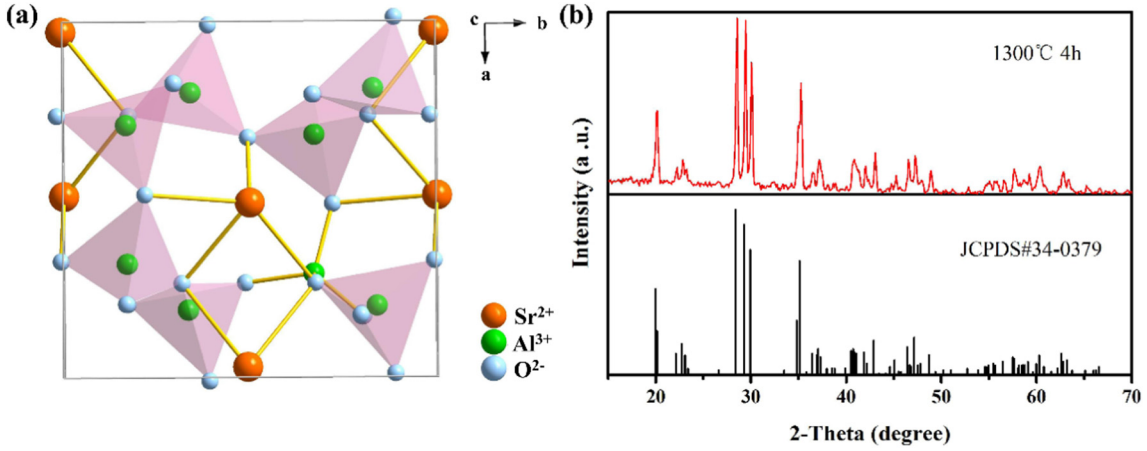

Fig. 1. (a) Crystal structure of $SrAl_2O_4$; (b) XRD patterns of SAOED and the standard data of $SrAl_2O_4$ host.

those of JCPDS-ICCD card (No. 34-0379), suggesting that SAOED single phase with monoclinic structure has been obtained in this work and the dopant of Eu^{2+} and Dy^{3+} shows no obvious change on the crystal structure.

The UV–vis absorption spectra of the SAOED samples with various doping concentration were measured as shown in Fig. S1. The absorption band from 200 to 400 nm is clearly observed for all samples, which could be ascribed to the host absorption. Another two absorption bands from 240 nm to 310 nm and from 310 nm to 500 nm should be attributed to the charge migration of $O^{2-} \rightarrow Eu^{2+}$ and the typical $4f^7 \rightarrow 4f^65d^1$ transition of Eu^{2+}, respectively [25]. The absorptions of characterized f-f transitions of Dy^{3+} (e.g., $^6H_{15/2} \rightarrow {}^4M_{15/2}$, $^6H_{15/2} \rightarrow {}^4K_{17/2}$, $^6H_{15/2} \rightarrow {}^4G_{11/2}$, $^6H_{15/2} \rightarrow {}^4I_{15/2}$) are suggested to be overlapped with the Eu^{2+} absorption bands from 330 nm to 475 nm [26].

When excited by a UV light, the SAOED samples could emit intense photoluminescence (PL) with green color. The PL excitation spectra of SAOED are depicted in Fig. 2a, which suggests the optimum excitation wavelength for SAOED locate at ca. 331 nm. The emission spectra of SAOED under the excitation of 331 nm are shown in Fig. 2b, which exhibits a broad band with maximum peak at ca. 519 nm, corresponding to d-f transitions of Eu^{2+} [23]. The PL intensity strongly depends on the doping contents, and $SrAl_2O_4$: 2% Eu^{2+}, 1% Dy^{3+} presents the highest emission intensity (Fig. S2).

It should be noted that SAOED could continuously emit light when the UV irradiation source was removed. The initial intensity of SAOED was very high and then the intensity of the afterglow decreased rapidly, and finally formed a stable long persistent emission [27]. Fig. 3 shows the decay characteristics of SAOED, tested by continuous exciting with a 365 nm UV light for about 15 min. The measurements started in the darkness after the excited source was cut off. The afterglow decay curve in Fig. 3 consists of fast decay period and slow decay period, corresponding to the short survival time of the electrons in Eu^{2+} and the deep trap energy center of Dy^{3+}, respectively [28]. When Eu^{2+} content was fixed, the increased concentration of Dy^{3+} could remarkably increase the initial intensity and decay time (Fig. 3a). When Dy^{3+} was fixed to 1%, there was no obvious change on the decay properties by varying the content of Eu^{2+} (Fig. 3b). For occlusal applications, the negative effect of afterglow of SAOED should be eliminated maximally. The SAOED samples with doping 1% Dy^{3+} and 1–4% Eu^{2+} in Fig. 3b show almost no afterglow after removing the irradiation source just for 20 s, satisfying the requirement of oral applications.

When varying the doping concentration of Eu^{2+} and Dy^{3+}, the ML properties of SAOED will be changed simultaneously because of the adjustment of the trap depth and concentration in structure [21]. Fig. 4 shows the ML spectra of SAOED samples by directly scratching the surface. For ML characterizations, the SAOED was composited with epoxy resin, and the scratch experiment was operated on a rotary tribometer (MS-T3001) to fix the rotational speed and normal force.

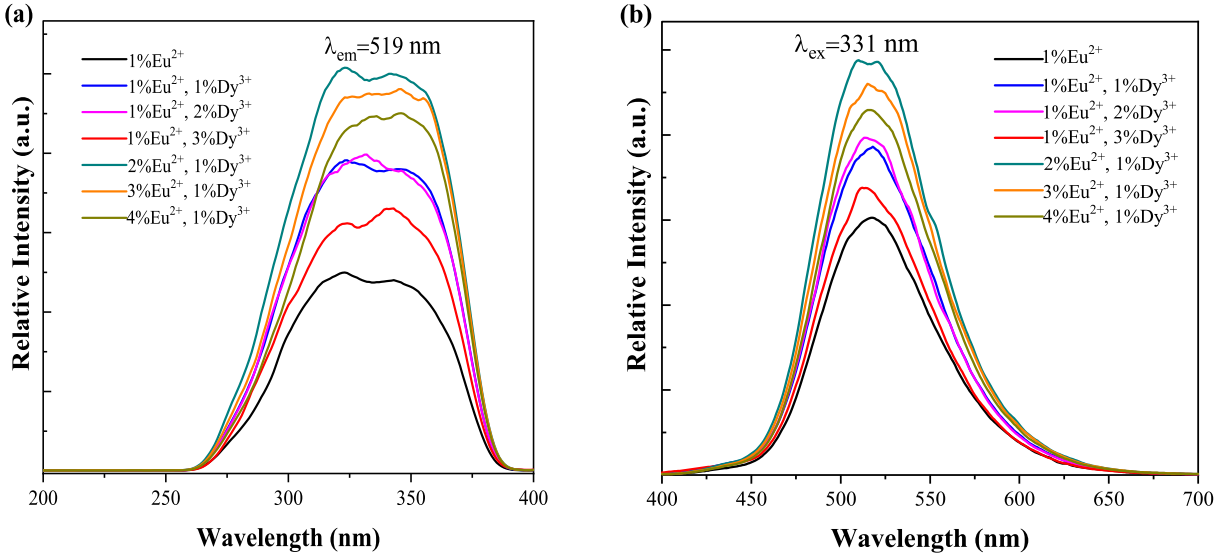

Fig. 2. (a) Excitation and (b) emission spectra of SAOED series monitored at 519 nm and excited by 331 nm, respectively.

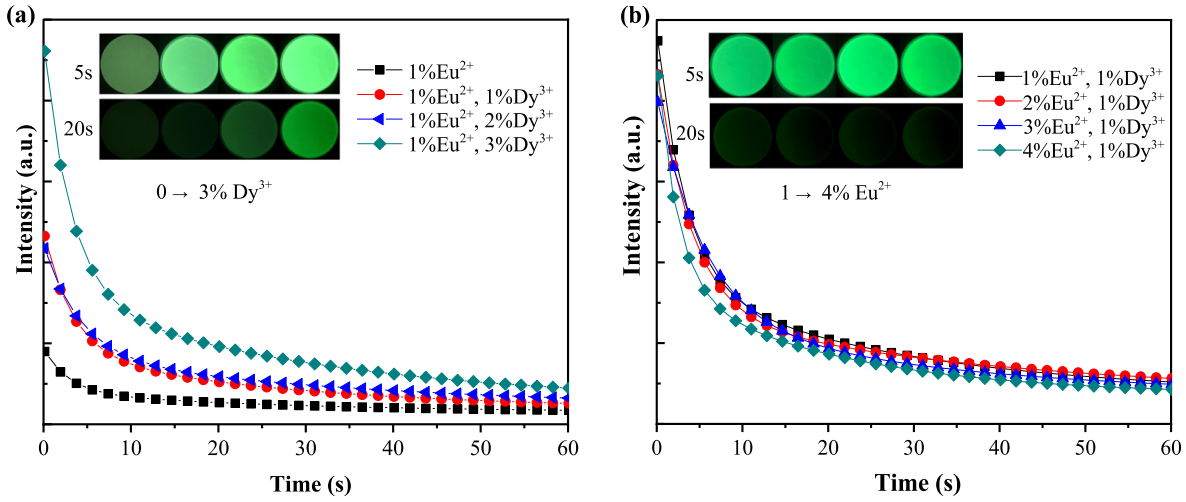

Fig. 3. The afterglow decay curves of SAOED samples with (a) different Dy^{3+} doping concentration (0%, 1%, 2%, 3%) and (b) different Eu^{2+} doping concentration (1%, 2%, 3%, 4%).

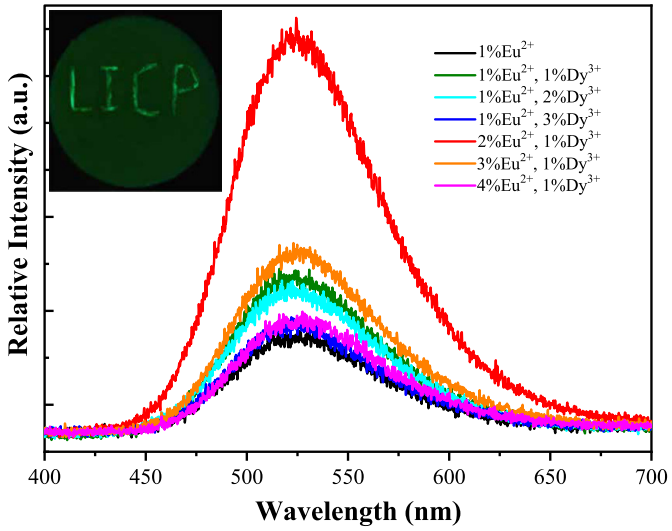

Fig. 4. Scratch induced ML spectra of SAOED/epoxy resin composites doped with various Eu^{2+} and Dy^{3+}.

The ML spectrum is same with the PL one, suggesting they possess the same emitting processes. It is observed in Fig. 4 that the ML intensity could be greatly affected by varying the doping concentration, and SAOED with doping 1% Dy^{3+} and 2% Eu^{2+} shows the highest ML intensity (Fig. S2) which could be clearly seen by naked eyes. Since $SrAl_2O_4$: 2% Eu^{2+}, 1% Dy^{3+} also shows a rapid decay of afterglow, it is confirmed to be the optimal sample for further occlusal applications.

In addition to scratch, the SAOED/epoxy resin composites could emit ML by mechanical compression, as is well-known that scratch and compression are ubiquitous in oral environment. Fig. 5a shows the compression induced ML spectrum of $SrAl_2O_4$: 2% Eu^{2+}, 1% Dy^{3+} under an applied load of 1000 N with a loading rate of 100 N/s. The ML of SAOED could be clearly observed as presented in the insets of Fig. 5. The ML intensity directly relates to the compressive load as shown in Fig. 5b. With increasing the compressive load from 0 N to 1000 N, the ML intensity is gradually increased. The one-to-one correspondence relationship in Fig. 5b suggests that the ML composites could be applied for mechanics detection. Moreover, it is reported that the maximum bite force of human jaw is ca. 600 N, confirming the optimized ML composites are appropriate for occlusal examination of artificial tooth [29].

To verify the idea for mechanics detection in artificial tooth, the optimized SAOED was further composited with commercial DBR. Fig. 6a and b show the friction coefficient, wear rate and shore A hardness of SAOED/DBR composites with various weight ratios. The above experimental values of DBR in Fig. 6 are close to the reported ones [30]. Moreover, it is found that the composition of SAOED could maintain the friction coefficient and hardness of DBR itself, while further improve its anti-wear ability. The reduced wear rate of the composites should be attributed to particle filling effect associated with the high strength of SAOED [31]. The sample with the SAOED to DBR weight ratio of 1:7 (S1-D7) showed the optimum performance with 28.7% decrease of the wear rate, which was chosen for ML characterization. Fig. 6c shows the ML spectrum of the SAOED/DBR composite with weight ratio of 1:7, stimulated by surface scratching. The bright ML from the composite confirms that DBR could act as a desirable elastic-supporter for ML generation.

As a widely used oral medical material, DBR is proved to possess a high level of biosecurity. Therefore, the biocompatibility of SAOED/DBR composite is the key that determines whether it is eligible for oral medical use. The viability and proliferation rate of L929 cells on DBR and SAOED/DBR composites were assessed by using the MTT assay [32]. Fig. 7 shows the proliferation of L929 cells on the surface of SAOED/DBR composites at 1, 2 and 4 days. It can be seen that comparing with the control group, there is no significant difference on the proliferation rate of each experiment group. Results illustrate that SAOED/DBR composite shows no cytotoxicity to L929 cells and is of a reliable biosecurity.

The mechanical, tribological, ML and biocompatible investigations suggest that the composition of SAOED in DBR is a feasible approach to realize the mechanics self-detection in artificial tooth. Herein, standard artificial tooth models were finally prepared based on SAOED/DBR composite with a weight ratio of 1:7 (Fig. 8a and b). With the introduction of SAOED in oral standard model, it exhibited bright green PL when excited by a 365 nm UV light as shown in Fig. 8c. When the models were scratched or rubbed, visible green emission can be directly observed by naked eyes as shown in Fig. 8d. Such behavior suggests that the stress concentration region of artificial tooth, like bulges on occlusal surface, would emit ML first during occlusal process. Moreover, the higher contact pressure would arouse brighter ML, which could guide clinicians to purposefully deal with the occlusal surface until a balanced occlusion established.

4. Conclusions

With varying the doping contents of Eu^{2+} and Dy^{3+}, the afterglow

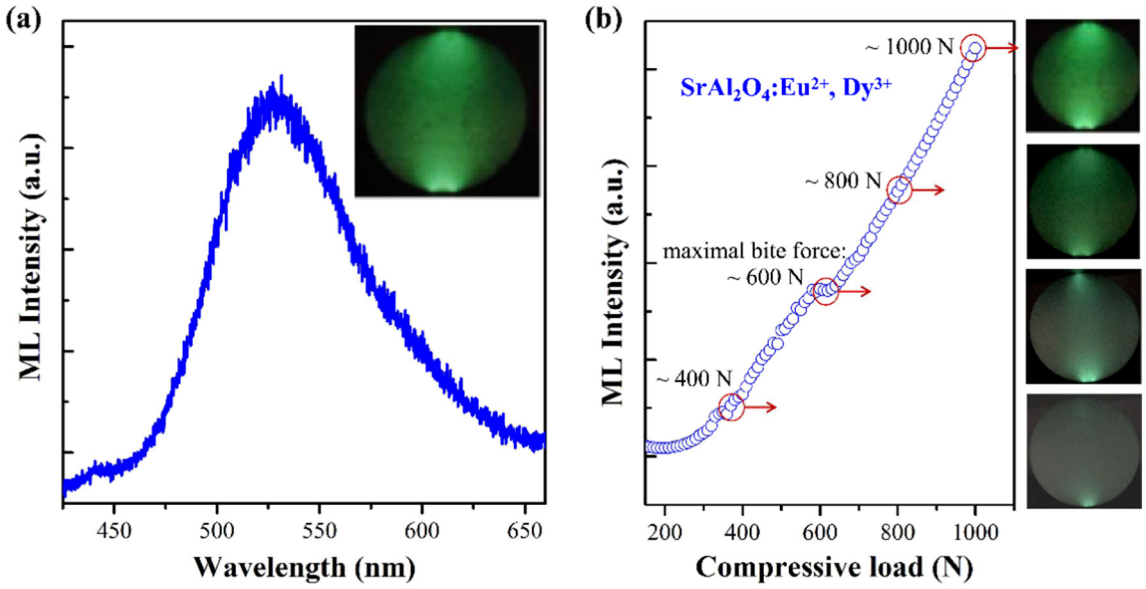

Fig. 5. (a) Compress induced ML spectrum of the $Sr_{1-x-y}Al_2O_4$: xEu^{2+}, yDy^{3+} ($x = 0.02$, $y = 0.01$)/epoxy resin composites under a compressive load of 1000 N; (b) ML intensity of the $Sr_{1-x-y}Al_2O_4$: xEu^{2+}, yDy^{3+} ($x = 0.02$, $y = 0.01$)/epoxy resin composites as a function of compressive load.

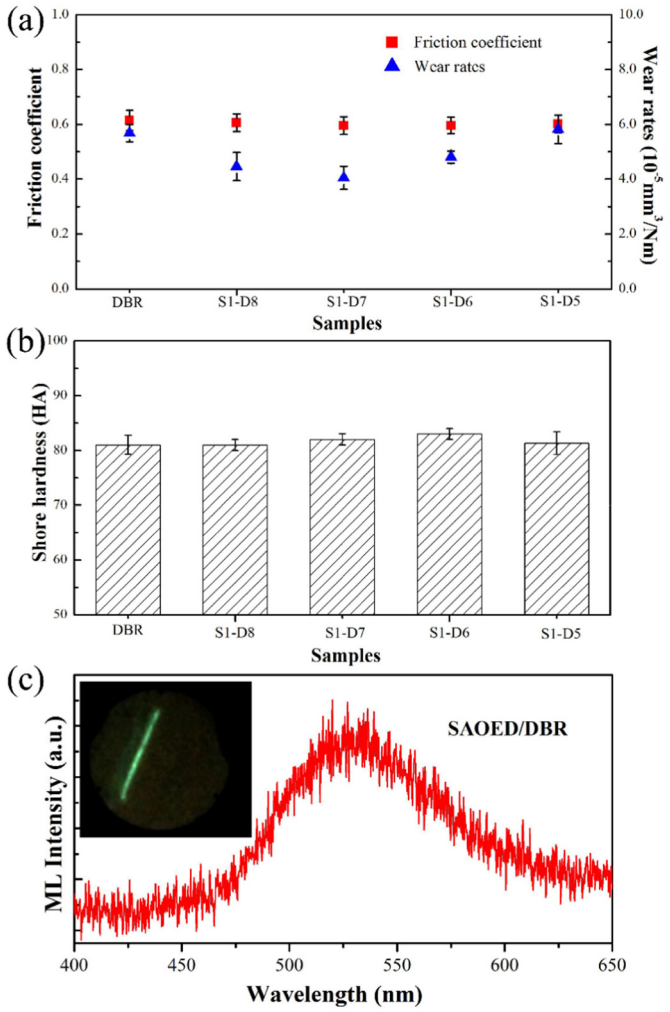

Fig. 6. (a) Tribology, (b) hardness and (c) scratch induced ML spectrum of $Sr_{1-x-y}Al_2O_4$: xEu^{2+}, yDy^{3+} ($x = 0.02$, $y = 0.01$)/DBR composites.

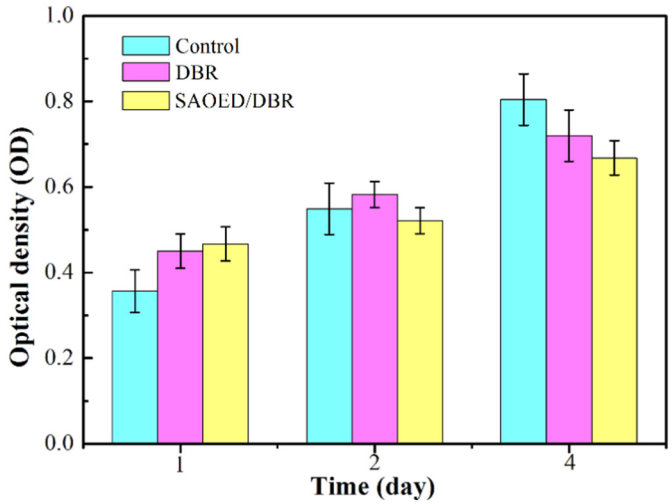

Fig. 7. Comparison optical density of L929 cells after being cultured with DBR and SAOED/DBR composite at 1, 2, and 4 days.

and ML properties of SAOED were adjusted, and SAOED with 2% Eu^{2+} and 1% Dy^{3+} was confirmed to be the optimal sample for the practical occlusal mechanics detection. After compositing with commercial DBR, luminescent characterizations suggest that DBR is an appropriate elastic-supporter for ML. In addition, the SAOED/DBR composites show good biocompatibility and enhanced mechanical properties, which are beneficial to oral medical applications. The direct observation of ML from the constructed standard oral models suggest it is an effective way to detect the mechanics in occlusal examination of artificial tooth, which could guide clinicians to purposefully deal with the occlusal surface to achieve occlusal balance.

Acknowledgments

This work is supported by the Natural Science Foundation of Gansu Province (17JR5RA319), the CAS Pioneer Hundred Talents Program, the National Natural Science Foundation of China (81571829), the Fundamental Research Funds for the Central Universities (lzujbky-2016-71), and the Natural Science Foundation of Gansu Province

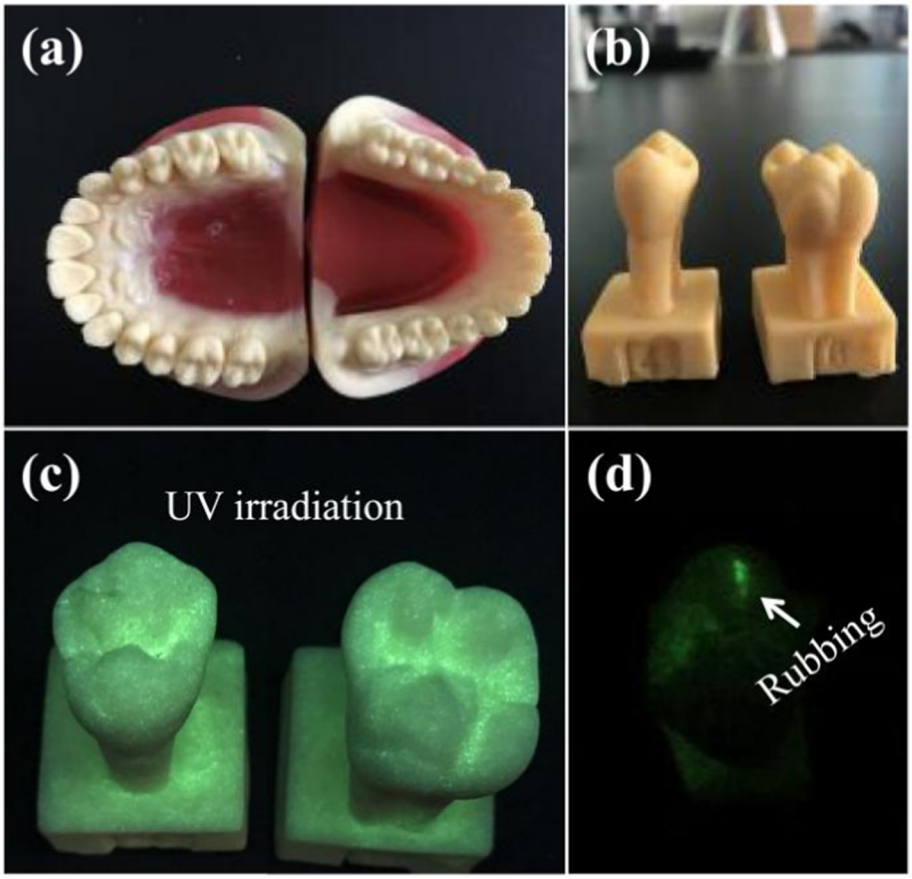

Fig. 8. (a, b) Photographs of SAOED/DBR composite fabricated artificial tooth; (c) PL and (d) ML images of the artificial tooth excited by UV light and rubbing, respectively.

(1610RJZA106).

Appendix A. Supplementary data

Supplementary data to this article can be found online at https://doi.org/10.1016/j.msec.2018.06.056.

References

[1] M. Bhola, L. Cabanilla, S. Kolhatkar, Dental occlusion and periodontal disease: what is the real relationship? J. Calif. Dent. Assoc. 36 (12) (2008) 924–930.
[2] C.M. De Felício, C.L.P. Ferreira, A.P.M. Medeiros, M.A.M.R. Da Silva, G.M. Tartaglia, C. Sforza, Electromyographic indices, orofacial myofunctional status and temporomandibular disorders severity: a correlation study, J. Electromyogr. Kinesiol. 22 (2) (2012) 266–272.
[3] S.S. Kimmel, Rationale and technique for achieving occlusal harmony, N. Y. State Dent. J. 75 (1) (2009) 39–43.
[4] D. Augusti, G. Augusti, D. Re, C. Dellavia, A.B. Giannì, Effect of different dental articulating papers on SEMG activity during maximum clenching, J. Electromyogr. Kinesiol. 25 (4) (2015) 612–618.
[5] A. Sharma, G.R. Rahul, S.T. Poduval, K. Shetty, B. Gupta, V. Rajora, History of materials used for recording static and dynamic occlusal contact marks: a literature review, J. Clin. Exp. Dent. 5 (1) (2013) e48.
[6] S. Qadeer, R. Kerstein, R.J.Y. Kim, J.-B. Huh, S.-W. Shin, Relationship between articulation paper mark size and percentage of force measured with computerized occlusal analysis, J. Adv. Prosthodont. 4 (1) (2012) 7–12.
[7] J.P. Carey, M. Craig, R.B. Kerstein, J. Radke, Determining a relationship between applied occlusal load and articulating paper mark area, Open Dent. J. 1 (1) (2007).
[8] R.B. Kerstein, J. Radke, Clinician accuracy when subjectively interpreting articulating paper markings, Cranio 32 (1) (2014) 13–23.
[9] M.N. Saad, G. Weiner, D. Ehrenberg, S. Weiner, Effects of load and indicator type upon occlusal contact markings, J Biomed Mater Res B Appl Biomater 85((1) (2008) 18–22.
[10] D. Hützen, P. Proff, T. Gedrange, R. Biffar, O. Bernhard, T. Kocher, B. Kordaß, Occlusal contact patterns–population-based data, Ann. Anat. 189 (4) (2007) 407–411.
[11] D. Peng, B. Chen, F. Wang, Recent advances in doped mechanoluminescent phosphors, ChemPlusChem 80 (8) (2015) 1209–1215.
[12] J.-C. Zhang, Y.-Z. Long, X. Yan, X. Wang, F. Wang, Creating recoverable mechanoluminescence in piezoelectric calcium niobates through Pr^{3+} doping, Chem. Mater. 28 (11) (2016) 4052–4057.
[13] Y. Zhang, G. Gao, H.L. Chan, J. Dai, Y. Wang, J. Hao, Piezo-phototronic effect-induced dual-mode light and ultrasound emissions from ZnS: Mn/PMN-PT thin-film structures, Adv. Mater. 24 (13) (2012) 1729–1735.
[14] S.M. Jeong, S. Song, S.K. Lee, N.Y. Ha, Color manipulation of mechanoluminescence from stress-activated composite films, Adv. Mater. 25 (43) (2013) 6194–6200.
[15] C.-N. Xu, T. Watanabe, M. Akiyama, X.-G. Zheng, Direct view of stress distribution in solid by mechanoluminescence, Appl. Phys. Lett. 74 (17) (1999) 2414–2416.
[16] C.-N. Xu, X.-G. Zheng, M. Akiyama, K. Nonaka, T. Watanabe, Dynamic visualization of stress distribution by mechanoluminescence image, Appl. Phys. Lett. 76 (2) (2000) 179–181.
[17] X. Wang, H. Zhang, R. Yu, L. Dong, D. Peng, A. Zhang, Y. Zhang, H. Liu, C. Pan, Z.L. Wang, Dynamic pressure mapping of personalized handwriting by a flexible sensor matrix based on the mechanoluminescence process, Adv. Mater. 27 (14) (2015) 2324–2331.
[18] S.M. Jeong, S. Song, K.-I. Joo, J. Kim, S.-H. Hwang, J. Jeong, H. Kim, Bright, wind-driven white mechanoluminescence from zinc sulphide microparticles embedded in a polydimethylsiloxane elastomer, Energy Environ. Sci. 7 (10) (2014) 3338–3346.
[19] W. Jia, H. Yuan, L. Lu, H. Liu, W. Yen, Phosphorescent dynamics in $SrAl_2O_4$: Eu^{2+}, Dy^{3+} single crystal fibers, J. Lumin. 76 (1998) 424–428.
[20] B. Chandra, C. Xu, H. Yamada, X. Zheng, Luminescence induced by elastic deformation of ZnS: Mn nanoparticles, J. Lumin. 130 (3) (2010) 442–450.
[21] J.-C. Zhang, L.-Z. Zhao, Y.-Z. Long, H.-D. Zhang, B. Sun, W.-P. Han, X. Yan, X. Wang, Color manipulation of intense multiluminescence from CaZnOS: Mn^{2+} by Mn^{2+} concentration effect, Chem. Mater. 27 (21) (2015) 7481–7489.
[22] T. Matsuzawa, Y. Aoki, N. Takeuchi, Y. Murayama, A. New Long, Phosphorescent phosphor with high brightness, $SrAl_2O_4$: Eu^{2+}, Dy^{3+}, J. Electrochem. Soc. 143 (8) (1996) 2670–2673.
[23] X. Xu, Y. Wang, X. Yu, Y. Li, Y. Gong, Investigation of Ce-Mn energy transfer in $SrAl_2O_4$:Ce^{3+}, Mn^{2+}, J. Am. Ceram. Soc. 94 (1) (2011) 160–163.
[24] R. Shi, M. Qi, L. Ning, F. Pan, L. Zhou, W. Zhou, Y. Huang, H. Liang, Combined experimental and ab initio study of site preference of Ce^{3+} in $SrAl_2O_4$, J. Phys. Chem. C 119 (2015) 19326–19332.
[25] D. Kshatri, A. Khare, Comparative study of optical and structural properties of micro- and nanocrystalline $SrAl_2O_4$: Eu^{2+}, Dy^{3+} phosphors, J. Lumin. 155 (2014) 257–268.
[26] U. Caldiño, A. Lira, A. Meza-Rocha, E. Pasquini, S. Pelli, A. Speghini, M. Bettinelli,

G. Righini, White light generation in Dy^{3+}- and Ce^{3+}/Dy^{3+}-doped zinc–sodium–aluminosilicate glasses, J. Lumin. 167 (2015) 327–332.
[27] J. Zhang, J. Lin, J. Wu, S. Zhang, P. Zhou, X. Chen, R. Xu, Preparation of long persistent phosphor $SrAl_2O_4$: Eu^{2+}, Dy^{3+} and its application in dye-sensitized solar cells, J. Mater. Sci. Mater. Electron. 27 (2) (2016) 1350–1356.
[28] H. Zhang, N. Terasaki, H. Yamada, C.-N. Xu, Development of mechanoluminescent micro-particles $Ca_2MgSi_2O_7$: Eu, Dy and their application in sensors, Thin Solid Films 518 (2) (2009) 610–613.
[29] J. Fastier-Wooller, H.P. Phan, T. Dinh, T.-K. Nguyen, A. Cameron, A. Öchsner, D.V. Dao, Novel low-cost sensor for human bite force measurement, Sensors 16 (8) (2016) 1244.
[30] V. Bavaresco, C. Zavaglia, M. Reis, J. Gomes, Study on the tribological properties of pHEMA hydrogels for use in artificial articular cartilage, Wear 265 (3) (2008) 269–277.
[31] A. Sepahvandi, M. Eskandari, F. Moztarzadeh, Fabrication and characterization of $SrAl_2O_4$: Eu^{2+} Dy^{3+}/CS-PCL electrospun nanocomposite scaffold for retinal tissue regeneration, Mater. Sci. Eng. C 66 (2016) 306–314.
[32] F. Song, W. Jie, T. Zhang, W. Li, Y. Jiang, L. Wan, W. Liu, X. Li, B. Liu, Room-temperature fabrication of a three-dimensional reduced-graphene oxide/polypyrrole/hydroxyapatite composite scaffold for bone tissue engineering, RSC Adv. 6 (95) (2016) 92804–92812.